Emergency Management
Science and Technology

ARTICLE

Open Access

https://doi.org/10.48130/emst-0024-0017
Emergency Management Science and Technology **2024**, 4: e016

Modeling and analysis of direct internal reforming in ethanol-fueled SOFC

Deivanayagam Hariharan[1], Bhaskar Sarkar[1,2] and Santhosh Gundlapally[1*]

[1] *Gamma Technologies, Westmont, IL-60559, USA*
[2] *Current: Shell International Exploration and Production Inc, Houston, TX-77082, USA*
* Corresponding author, E-mail: s.gundlapally@gtisoft.com

Abstract

Solid oxide fuel cells (SOFCs), in which the chemical energy of the fuel is directly converted to electrical energy, offer a compelling alternative to combustion-based power technologies due to their fuel flexibility, high efficiency, and low emissions, especially when coupled with combined heat and power (CHP) systems. SOFCs hold significant promise due to their potential to serve as distributed power sources and as reliable backup solutions during primary power disruptions. Among the various configurations of SOFC systems, those employing direct internal reforming stand out. This approach involves the *in-situ* conversion of hydrocarbon fuels like methane and diesel into hydrogen inside an SOFC device, which is subsequently electrochemically oxidized to generate power. This method offers distinct advantages over other configurations. In this study, a newly developed model is introduced that is specifically tailored for SOFCs with direct internal reforming of ethanol. By comparing the model's predictions with experimental data, its accuracy and reliability was validated. Additionally, a comprehensive analysis of polarization curves under varying operating conditions were conducted, examining factors such as hydrogen yield and species distribution along the channel length. This investigation enhanced our understanding of the internal reactions within SOFCs, providing valuable insights for optimizing their technology.

Citation: Hariharan D, Sarkar B, Gundlapally S. 2024. Modeling and analysis of direct internal reforming in ethanol-fueled SOFC. *Emergency Management Science and Technology* 4: e016 https://doi.org/10.48130/emst-0024-0017

Introduction

Climate change and global warming are major concerns for countries worldwide, prompting the adoption of various measures to decrease carbon emissions. One such measure is the utilization of carbon-free fuel, such as hydrogen. Oxidizing hydrogen fuel with air produces only water as a byproduct. Thus, hydrogen fuel has the potential to eliminate carbon emissions and other harmful combustion products such as oxides of sulfur (SOx) and volatile organic compounds (VOC). Hydrogen is being aggressively consumed by industries such as transportation, power generation, chemical and industrial operations, fuel blending, and others. One of the most important applications of hydrogen during the last decade is in fuel cells for power generation. In a fuel cell, chemical energy is directly converted into electrical energy without combustion with just water as a byproduct. Fuel cells have a simplex nature resulting in an electrical efficiency of over 60% with minimal to no emissions compared to combustion engines[1]. Among the many types of fuel cells, solid oxide fuel cells (SOFC) are promising due to their fuel flexibility, low operating costs, and high electrical efficiency. Furthermore, SOFCs do not require precious metals or corrosive acids, unlike other types of fuel cells such as proton exchange membrane fuel cells (PEMFCs), Phosphoric acid fuel cells (PAFCs), and Direct methanol fuel cells (DMFCs).

SOFCs consist of a ceramic electrolyte, a cathode, and an anode. Oxygen is reduced in the cathode, forming oxygen ions that then diffuse through the solid electrolyte to the anode, where they oxidize the fuel. The ceramic material needs an extremely high temperature (> 500 °C) to conduct oxygen ions. SOFCs can be classified into two types based on how fuel is reformed: internal reforming SOFCs (DIR-SOFCs) and external reforming SOFCs. In external reforming SOFCs, hydrocarbon fuels are reformed outside the fuel cell in a separate reactor to produce hydrogen, which is then directed to the anode of the fuel cell. In DIR-SOFCs, hydrocarbon fuels are directly supplied to the anode, and reforming primarily takes place in the anode support layer. The ability to utilize a diverse range of conventional fuels expands the application of SOFCs because it eliminates the need for pure hydrogen as required by low temperature fuel cells such as PEMFCs.

In comparison to SOFCs with external reformers, DIR-SOFCs offer significant advantages such as improved thermal management, faster response time, simplicity, and compactness. These benefits stem from the direct supply of hydrocarbon fuels to the anode, where reforming primarily occurs within the anode support layer. This integrated approach not only simplifies the system architecture but also enhances overall efficiency and performance, making DIR-SOFCs a compelling choice for a wide range of applications.

One of the major obstacles in the worldwide adoption of hydrogen as a fuel is its lack of availability in a pure form. However, besides the traditional method of reforming conventional fuels to produce hydrogen, there are also alternative renewable sources like solar, wind, and e-fuels that make hydrogen a viable and eco-friendly option. Nonetheless, it is important to understand the practicality of meeting the increasing demand for hydrogen fuel. In 2021[2], global hydrogen production reached 94 million tons (Mt H_2), with the majority derived from natural gas (~62%) and coal. Only 0.04% of the

hydrogen was derived from fossil-free sources through water electrolysis and the associated emissions for this production were more than 900 Mt of CO_2. To maintain the overall effectiveness of hydrogen fuel in reducing greenhouse gas emissions, the dependence on fossil fuels in its production process needs to be significantly reduced. Aside from electrolysis, alternative sources for producing clean hydrogen include biowaste and biofuels. However, all these sources significantly increase the cost of hydrogen. Hydrogen is categorized into various colors based on the energy sources for its production, ranging from black/brown to white[3,4].

To be cost-effective and phase out fossil fuel dependence, renewable fuels, such as ethanol, are promising methods. Ethanol is readily available owing to its increasing use as a blending agent with gasoline, making it an ideal candidate for producing hydrogen through reforming. The US produces 17.5 billion gallons of ethanol per year as of 2021[5]. Although reforming methane/methanol has been extensively studied for decades, ethanol reforming to produce hydrogen is more attractive due to its less toxic nature. Ethanol can be converted into hydrogen through thermochemical, hydrothermal, photochemical, and electrochemical processes[6], among which steam reformation of ethanol to produce hydrogen, a thermochemical process, is the focus of the current work. Steam reforming is a widely used process due to its efficiency and versatility in utilizing various hydrocarbons and a wide range of operating temperatures.

Steam reforming is an endothermic process that involves reacting hydrocarbons, like methane or ethanol, with steam to produce syngas, a mixture of hydrogen and carbon monoxide. Catalysts are typically used to enhance the thermal breakdown of hydrocarbons during steam reforming. Noble metals, such as platinum (Pt) or rhodium (Rh), are excellent catalysts for low-temperature reforming to produce hydrogen. However, transition metals such as nickel (Ni) are often used in applications where temperatures greater than 600 °C due to their cost-effectiveness[7]. Additionally, researchers have discovered that bimetallic catalysts containing noble metals, such as cerium oxide, result in a higher hydrogen yield when producing hydrogen from ethanol[8]. One of the major challenges of steam reforming is coking, a process that creates solid carbon (known as coke) when hydrocarbons are reformed with little to no oxidizing agent. Coking deactivates the catalyst by depositing on its surface and prevents the reformation process. To prevent coking, high operating temperatures[9,10] and a suitable steam-to-carbon molar ratio of between 3 and 5[11–15] are recommended.

Despite natural gas's current dominance in hydrogen production, ethanol's potential as an alternative source has been studied by various researchers. In particular, bioethanol has substantial benefits over methane/natural gas and should be explored further as a source fuel in hydrogen generation to meet current global warming targets. Furthermore, unlike methane, under specific operating conditions, the high temperature needs of ethanol reformation could be avoided. Garcia et al.[16] developed a model for reforming ethanol into acetaldehyde and subsequently hydrogen using SnO_2 and Co (Fe)/ZnO catalysts. The model has been validated using experimental data and can estimate the required inputs and operating conditions to produce enough H_2 to feed a 1 kW proton-exchange membrane (PEM) fuel cell. Ulejczyk et al.[17] employed a similar cobalt-based catalyst in a plasma catalytic reactor to produce hydrogen from ethanol at temperatures ranging from 250 °C to 450 °C (523 to 723 K).

Ni et al.[18] evaluated the work of many researchers on bioethanol reformation in hydrogen generation. The authors identified Rh and Ni as the best and most often utilized steam reforming catalysts, with MgO, ZnO, CeO_2, and La_2O_3 as appropriate support components. López et al.[19] published a comprehensive study on the production, characterization, and reaction assessment of structured catalysts used in ethanol steam reforming to produce hydrogen. Through mathematical modeling, the authors also established activation energy and pre-exponent multipliers for the four main reactions that capture the ethanol steam reforming process. This work served as the foundation for the ethanol reformer modeling in this study, and their experimental data is being utilized to validate our ethanol reformer model predictions.

Several studies have investigated the suitability of different fuels in SOFCs. Andersson et al.[20] used a computational fluid dynamics-based model to examine the impact of multiple renewable fuels, including ethanol on SOFCs. The authors determined that ethanol is one of the sustainable fuels in a SOFC system. In another study, Dokmaingam et al.[21] developed a mathematical model to analyze the influence of various primary fuels, including ethanol, on internal reforming SOFCs and discovered that co-flow patterns with a finer temperature gradient along the system worked better.

Laosiripojana & Assabumrungrat[22] determined that the Ni/YSZ catalyst is well suited for methane and methanol as the primary fuel, but not ethanol in a direct internal reforming SOFC (DIR-SOFC), due to the catalyst's rapid degradation by carbon deposition even at high steam content and operating temperatures. In contrast, Augusto et al.[23] studied the Ni/GDC catalyst and determined its ability to operate with dry ethanol for 50 h without carbon production. Despite the economic advantages of nickel-based catalysts, nickel-free anodes have been employed in SOFC for fuels such as methane and ethanol. Finally, Sarruf et al.[24] evaluated the impact of bimetallic cells (ceria-Co-Cu) with monometallic cells (ceria-Co and ceria-Cu) and exhibited over 24 h of continuous operation without coking. The examination of literature on both internal and external reforming SOFCs were vital for contextualizing this study and comprehensively understanding the range of reforming approaches, along with their respective advantages and limitations. By reviewing existing research, the aim was to identify gaps in the literature and delineate areas where further investigation is warranted.

First, a detailed mathematical model that includes diffusion in the catalyst/wash coat layer of a monolith reactor was developed and validated against the measurements for ethanol steam reforming[25]. This model was used to study the effect of different operating conditions on the ethanol conversion and the production of H_2 along with other species such as CH_4, CO, and CO_2. Building on that, in this work, an SOFC model with direct internal reforming of ethanol and electrochemical oxidation of H_2 was developed and calibrated using a polarization curve measurements obtained from the literature[26]. Finally, the SOFC model was used to study the performance of SOFC under different operating conditions along with a discussion of the key characteristics observed in the behavior of different reacting species.

Internal reforming reactions

An ethanol reformer model was developed and validated[25] with the experimental measurements from López et al.[19]. The reforming mechanism consists of the following three reactions:

$$C_2H_5OH \rightarrow CH_4 + H_2 + CO \quad \Delta H = 49.3\ kJ/mol \qquad R1$$
$$CO + H_2O \rightleftharpoons CO_2 + H_2 \quad \Delta H = -41.16\ kJ/mol \qquad R2$$
$$CH_4 + H_2O \rightleftharpoons 3H_2 + CO \quad \Delta H = 206.17\ kJ/mol \qquad R3$$

The optimized activation energy and pre-exponential factors are reported in Table 1.

Where p_x corresponds to the partial pressure of the corresponding species and K_{eq} is the equilibrium constant. For additional details on the chemical kinetics, please refer to Hariharan et al.[25].

Figure 1 shows the model validation for ethanol conversion and H_2 yield for different reactor temperatures. Ethanol conversion reaches 100% above 700 K, whereas hydrogen yield increases linearly until 700 K, primarily from ethanol decomposition. From 700 and 850 K, a marginal increase in H2 yield occurs which is due to the WGS reaction, followed by a sharp increase from methane reforming reactions. The model was also able to capture all species mole fractions for the entire operating temperature range of 500 to 1,000 K.

Table 1. Global reaction rate expressions for the three reactions of ethanol reforming.

Reactions	Reaction rate expression (mol/m^3/s)
$C_2H_5OH \rightarrow CH_4 + H_2 + CO$	$716.67 * \exp\left(-\frac{87}{RT}\right) * p_{C_2H_5OH} * \rho_{cat}$
$CO + H_2O \rightleftharpoons CO_2 + H_2$	$6 * \exp\left(-\frac{70}{RT}\right) * \left((p_{CO} * p_{H_2O}) - \frac{(p_{CO_2} * p_{H_2})}{K_{eq2}}\right) * \rho_{cat}$
$CH_4 + H_2O \rightleftharpoons 3H_2 + CO$	$8833.33 * \exp\left(-\frac{162}{RT}\right) * \left((p_{CH_4} * p_{H_2O}) - \frac{(p_{CO} * p_{H_2}^3)}{K_{eq3}}\right) * \rho_{cat}$

Model setup for SOFC

An SOFC model with direct internal reforming of ethanol was developed based on the validated kinetics of ethanol reformer model as shown in Fig. 2. A schematic representation of the two-stage process of reforming ethanol to hydrogen and then to power with water as a byproduct is shown in Fig. 3. Laminar flow is assumed in the channel as the Reynolds numbers encountered in the fuel cells are less than 2,000 even at the highest current densities and the flow is assumed to be fully developed. Additionally, the axial diffusion in the channel is assumed negligible as flow is dominated by convection and radial diffusion in the channel is accounted for using the widely used mass transfer coefficient approach[27].

The governing equation of species concentrations in both the anode and cathode channels is given by:

$$\frac{\partial \omega_{g,j}}{\partial t} = -u\frac{\partial \omega_{g,j}}{\partial z} - k_{me,j} S_{flux}\left(\omega_{g,j} - \omega_{s,j}\big|_{y=0}\right) \qquad (1)$$

where, S_{flux} is the specific surface area defined as the ratio of interfacial surface area to the flow volume, $S_{flux} = \frac{A_s}{V_f}$. Since mass

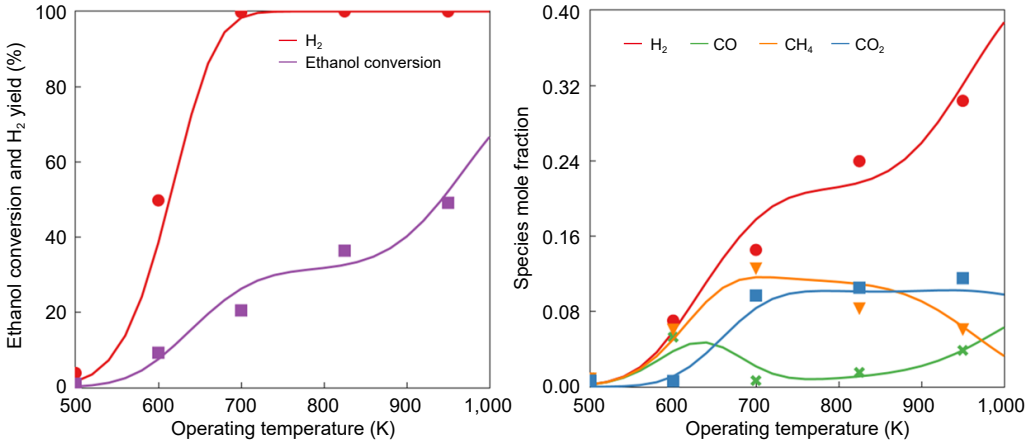

Fig. 1 Model validation on the effects of various operating temperatures on (a) ethanol conversion and H_2 yield, and (b) species mole fraction (lines represent the model results and the dots represent experimental measurements from López et al.[19]).

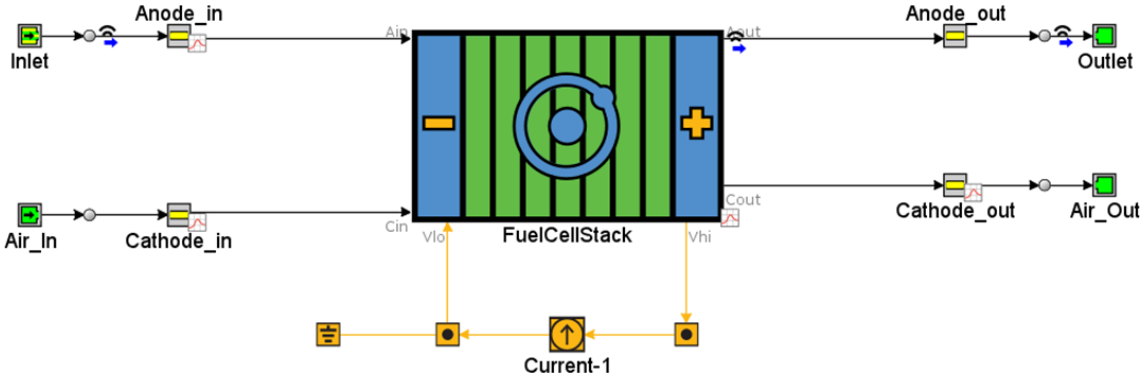

Fig. 2 GT-SUITE model for direct reforming ethanol SOFC.

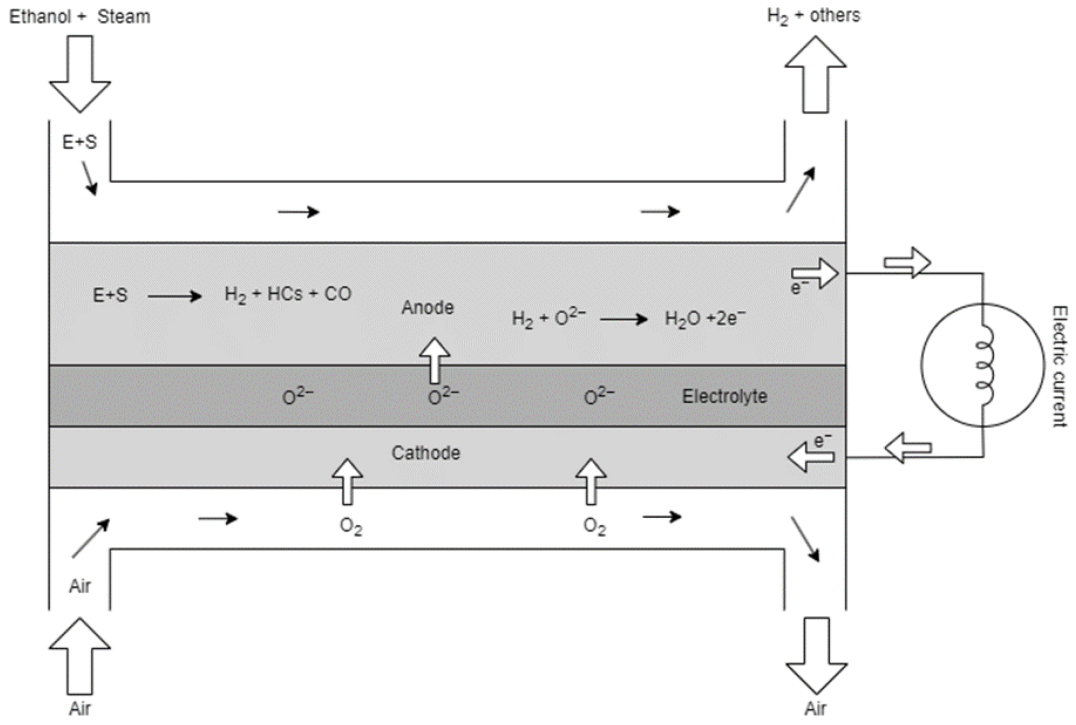

Fig. 3 Schematic diagram of direct reforming ethanol SOFC.

transfer from the channel to the diffusion layers occurs through only one wall of the flow channel, Sherwood number assumes different value than that of external reformers where all four channel walls are open to mass transfer; its values as function of aspect ratio are taken from Shah & London[28], and shown in Table 2.

The governing reaction-diffusion equation for species balance in the anode support layer is:

$$\frac{\mathrm{d}\omega_{\mathrm{s,j}}}{\mathrm{dt}} = \frac{1}{\epsilon_s \rho_s}\left[\mathrm{D_{s,j}}\rho_s \frac{\partial^2 \omega_{\mathrm{s,j}}}{\partial \mathrm{y}^2} + \mathrm{R_{s,j}}\right] \tag{2}$$

with the boundary condition given as:

$$-\mathrm{D_{s,j}}\rho_s \frac{\partial \omega_{\mathrm{s,j}}}{\partial \mathrm{y}}\bigg|_{\mathrm{y=0}} = \mathrm{k_{me,j}}\rho_{\mathrm{g}}\mathrm{S_{flux}}\left(\omega_{\mathrm{g,j}} - \omega_{\mathrm{s,j}}\big|_{\mathrm{y=0}}\right) \tag{3}$$

$$-\mathrm{D_{s,j}}\rho_s \frac{\partial \omega_{s,j}}{\partial y}\bigg|_{y=\delta} = \mathrm{R_{ct}} \tag{4}$$

These equations account for the simultaneous diffusion and reactions within the anode support layer and the charge transfer reactions. $R_{s,j}$ is the volumetric species production rate of species j due to chemical reactions, where the volume basis is anode support layer volume, V_s. R_{ct} is the area-specific species production rate due to electrochemical reactions, where the area basis is the electrochemically active surface area, A_{CT}. The anode support layer (solid phase) volume is calculated as, $V_s = A_s \delta_s N_{cells}$, where A_s is the geometric surface area of a single anode support layer, which is also used to convert current to current density. In the present implementation, A_s is also used in the calculation of the total electrochemically active surface area, A_{CT}, i.e., $A_{CT} = A_s N_{cells}$.

Table 2. Sherwood number as a function of aspect ratio.

Aspect ratio	0.2	0.4	0.7	1.0	2.0	2.5	5.0	10.0
Sh	0.96	1.60	2.26	2.71	3.54	3.78	4.41	4.85

The effective diffusivities are calculated as follows:

$$\mathrm{D_{s,j}} = \frac{\tau}{\varepsilon_s}\left(\frac{1}{\mathrm{D_{f,j}}} + \frac{1}{\mathrm{D_{kn,j}}}\right)^{-1} \tag{5}$$

$$\mathrm{D_{kn,j}} = \frac{\mathrm{d_p}}{3}\sqrt{\frac{8\mathrm{RT_s}}{\pi \mathrm{MW_j}}} \tag{6}$$

where, $D_{f,j}$ denotes the bulk diffusivity and $D_{kn,j}$ is the Knudsen diffusivity of species j. The porosity and tortuosity of the porous anode layer are given by ε_s and τ, respectively, and d_p denotes the pore diameter.

Alternatively, the effect of diffusional limitations on voltage output can be considered by an empirical approach as described in later sections. In the limit of negligible diffusional limitation, (Eqn 2) can be integrated along with the boundary conditions to obtain the following form:

$$\frac{\mathrm{d}\omega_{\mathrm{s,j}}}{\mathrm{dt}} = \frac{1}{\varepsilon_s \rho_s}\left[\mathrm{k_{me,j}}\rho_{\mathrm{g}}\frac{\mathrm{A_{flux}}}{\mathrm{V_s}}\left(\omega_{\mathrm{g,j}} - \omega_{\mathrm{s,j}}\right) + \mathrm{R_{s,j}} + \mathrm{R_{CT}}\frac{\mathrm{A_{CT}}}{\mathrm{V_S}}\right] \tag{7}$$

Once the species concentration fields are calculated with the above equations following the similar numerical solution approaches reported previously[29,30] for a specified current density, SOFC voltage output is calculated by subtracting different voltage losses from the theoretical reversible cell voltage. It is known that oxidation of both H_2 and CO species can contribute to the charge transfer:

$$\mathrm{CO} + 1/2\,\mathrm{O_2} \rightarrow \mathrm{CO_2} \quad \mathrm{R4}$$
$$\mathrm{H_2} + 1/2\,\mathrm{O_2} \rightarrow \mathrm{H_2O} \quad \mathrm{R5}$$

However, it is reported that the electrochemical oxidation of H_2 is about 10 times faster than that of CO. As a result, most of the CO is consumed indirectly *via* water gas shift reaction which converts CO to H_2. Jiang & Virkar[31] investigated different ratios of CO/H_2 and reported that even with 55% of CO in the mixture of H_2 and CO, the performance of the cell was only

slightly different from pure H_2, since most of the CO undergoes the WGS reaction with the available water. Conversely, when enough water is in the mixture, which is true for the steam reforming of ethanol, charge transfer predominantly occurs *via* H_2 oxidation reaction. Thus, in this work, the H_2 oxidation reaction only was considered as this considerably simplifies voltage loss calculations.

The output voltage of the SOFC is calculated by subtracting different losses from the theoretical voltage calculated by the Nernst equation:

$$V = V_{Nernst} - \eta_{act,a} - \eta_{act,c} - \eta_{ohmic} - \eta_{conc,a} - \eta_{conc,c} \quad (8)$$

Each term in the above equation is discussed next. Nernst potential is calculated by the Gibbs free energy of formation of species involved in the hydrogen reaction as:

$$V_{Nernst} = -\frac{\Delta G_{rxn}}{2F} = -\frac{\Delta G_{f,H_2O} - \Delta G_{f,H_2} - 0.5\Delta G_{f,O_2}}{2F} \quad (9)$$

where, ΔG_f is the Gibbs free energy of a species at a given temperature and pressure. A more familiar form of the Nernst equation involving partial pressures can be obtained by assuming ideal gas and by using the relationship between Gibbs energy and species partial pressures:

$$\Delta G_f = \Delta G_f^0 + RT\ln(P/P_0) \quad (10)$$

Substituting the above equation in Eqn 9 gives the Nernst equation in terms of partial pressures of species:

$$V_{Nernst} = E^0 - \frac{RT}{2F}\ln\left(\frac{P_{H_2O}}{P_{H_2}P_{O_2}^{1/2}}\right) \quad (11)$$

Activation loss, η_{act} represents voltage loss due to charge transfer reactions and it is calculated for both anode and cathode using the Butler-Volmer equation:

$$i = i_0\left[\exp\left(\frac{\alpha F\eta_{act}}{RT}\right) - \exp\left(\frac{-(1-\alpha)F\eta_{act}}{RT}\right)\right] \quad (12)$$

where, i is current density, i_0 is exchange current density, and α is charge transfer coefficient. The anodic and cathodic exchange current densities are calculated using the following equations:

$$i_0^{an} = \gamma^{an}\left(\frac{p_{H_2}^*}{p_{ref}}\right)^a\left(\frac{p_{H_2O}^*}{p_{ref}}\right)^b\exp\left[-\frac{E_a^{an}}{RT}\right] \quad (13)$$

$$i_0^{ca} = \gamma^{ca}\left(\frac{p_{O_2}^*}{p_{ref}}\right)^c\exp\left[-\frac{E_a^{ca}}{RT}\right] \quad (14)$$

Voltage losses due to concentration polarization are implicitly accounted for when the full reaction-diffusion equation is solved, whereas they need to be explicitly calculated when the simplified equation given by (Eqn 7) is used in the support layer. The following function is widely used to calculate the concentration polarization,

$$V_{mt} = -C \times \ln\left(1 - \frac{i}{i_l}\right) \quad (15)$$

where, C represents the mass transport loss coefficient and i_l is the limiting current density. They are related to physical variables as:

$$C = \frac{RT}{nF}\left(1 + \frac{1}{\alpha}\right) \quad (16)$$

$$i_l = \frac{C_b D_e}{\delta} \quad (17)$$

However, it is known that the theoretical limiting current density calculated using the above relations yields much higher current densities than the measured values as the additional resistances such as surface diffusion of adsorbed species on the catalysts can contribute to the voltage loss. Surface diffusion is a highly localized phenomenon, and it is difficult to separate it from kinetics resistance. Considering this, C and i_l are often treated as model parameters and they are tuned to fit the experimental data. Using the above empirical approach reduces computational time as this avoids the discretization of the reaction-diffusion equation in the support layer and hence this can be useful when calibrating kinetics parameters of reforming reactions. Once good baseline values are obtained for kinetics parameters, the full solution can be used instead of the simplified solutions as used in this work.

Ohmic losses are calculated as:

$$\eta_{ohmic} = i \times ASR \quad (18)$$

where, ASR represents the area species Ohmic resistance, which predominantly depends on the conductivity of the electrolyte. Conduction of oxygen ions in the YSZ electrolyte takes place *via* the hopping mechanism and is an activated process with an activation temperature of about 10,300 K (activation energy of about 85 kJ/mol)[32]. Conductivity is evaluated by using an Arrhenius expression as:

$$\sigma = \sigma_0\exp\left[-\frac{10300}{T}\right] \quad (19)$$

$$ASR = \frac{1}{\sigma} \quad (20)$$

Results and discussion

In this section the results from several exploratory simulations carried out are presented and discussed with the aim of analyzing the effect of different operating conditions on the internal reforming and voltage performance. The reaction mechanism calibrated in the previous section is used in SOFC direct internal reforming model without any changes. Fuel cell performance related parameters, such as activation losses, ohmic resistance, and mass transfer losses, are calibrated to match the ethanol reforming results reported by López et al[19]. Figure 4 shows the comparison between the model and measurements for the voltage and power density. The polarization curve shows characteristics typical for a high-temperature SOFC: negligible activation losses but dominating ohmic losses due to oxygen ion conduction in the electrolyte.

Figure 5 shows the effect of operating temperature on the polarization curve. Hydrogen yield is higher at high temperatures. Nernst voltage is lower at high temperatures and hence voltage is lower for high temperatures at very low current densities (< 0.1 A/cm^2). At higher current densities (> 0.1 A/cm^2), high temperature leads to better performance due to lower activation and ohmic losses. It can be seen that performance improvement at high temperatures is primarily due to a large reduction in ohmic resistance.

The effect of current density on species mole fraction at the anode outlet for 700 °C is presented in Fig. 6. Hydrogen fraction reduced linearly with current density as expected due to the Faradaic relationship which relates to molar consumption of H_2 flux to be linearly related to the current density. As H_2 is consumed, CO fraction reduces, and CO_2 fraction increases because the water gas shift reaction converts CO to H_2 and CO_2. Meanwhile, CH_4 concentration remains almost the same

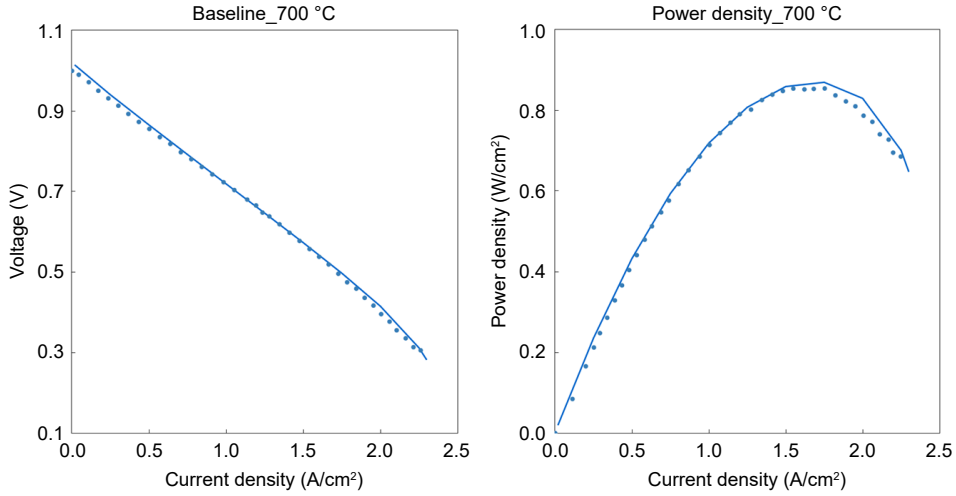

Fig. 4 The polarization curves of the fuel cell (lines represent the model results and the dots represent data from Dogdibegovic et al.)[26].

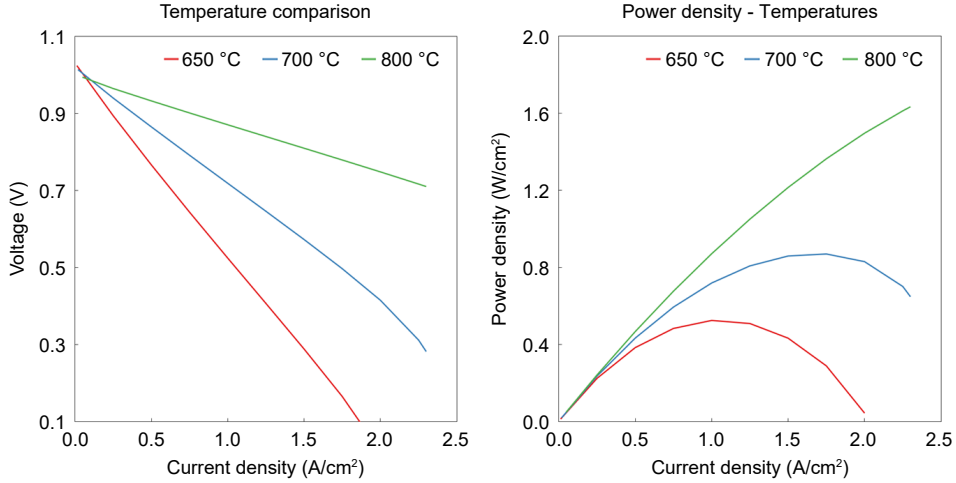

Fig. 5 Effect of current density on both the voltage and power density at 650 °C, 700 °C, and 800 °C.

because reaction 3 doesn't take place significantly at this temperature.

The current density and thermodynamic voltage potential across the fuel cell are presented in Fig. 7. It can be observed that the current density and voltage increase up to 0.25 (25% of the volume) and then start to decrease for 700 °C and slightly earlier for 800 °C. This is mainly because, unlike the fuel cells running with hydrogen, there is no hydrogen present at the entrance of the anode side of the fuel cell. The initial increase in the 25% is due to the reformation of ethanol to produce H_2, which is then oxidized in the anode to meet the current demand. This phenomenon is evident in the molar fraction of species across the length of the fuel cell, as depicted in Fig. 8. The molar fraction of ethanol decreases significantly up to 0.3 due to decomposition reactions, resulting in the production of CH_4, CO, and H_2. Subsequently, the water-gas shift (WGS) reaction and methane steam reforming (MSR) reactions come into play, utilizing available steam to generate more H_2 along with CO and CO_2. This trend is clearly illustrated in Fig. 8, where H_2, CO, and CO_2 consistently increase up to 0.25. Beyond this point, most of the ethanol has already decomposed, causing a decline in H_2 production from ethanol. Additionally, H_2 is continuously oxidized to produce H_2O and power output, resulting in an overall decrease in H_2 and an increase in H_2O. CO exhibits a similar trend as H_2, as the WGS reaction progresses in the forward direction due to the electrochemical oxidation depleting H_2.

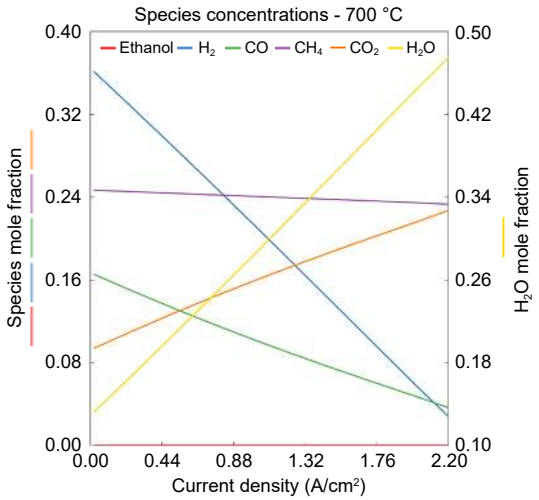

Fig. 6 Effect of current density on the species mole fraction for the 700 °C case.

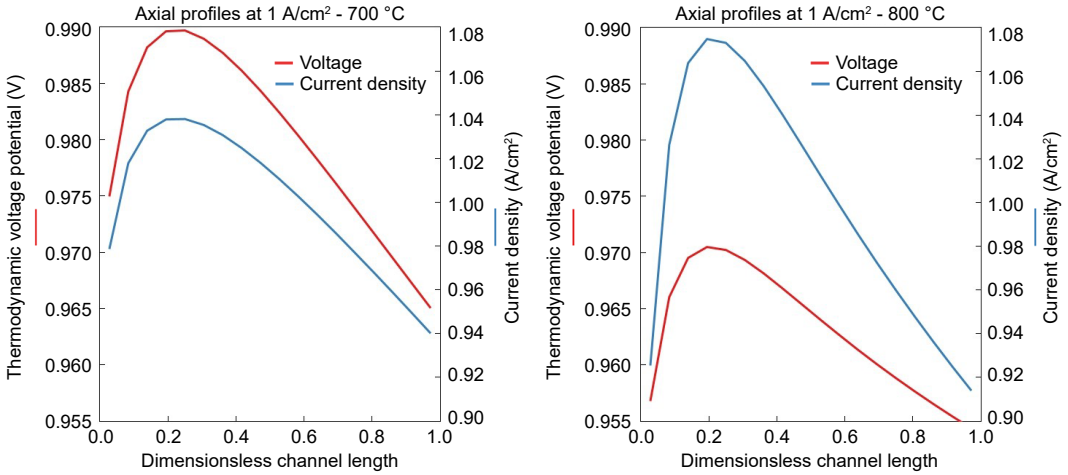

Fig. 7 Current density and thermodynamic voltage potential along the axis of SOFC at the operating temperatures of (a) 700 °C and (b) 800 °C.

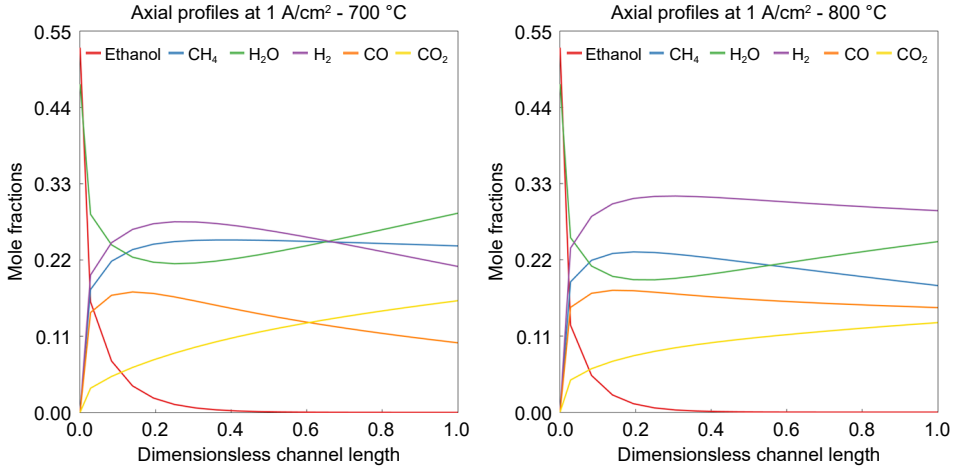

Fig. 8 Mole fractions of species along the axis of SOFC at the operating temperatures of (a) 700 °C and (b) 800 °C.

When comparing the CH_4 concentration at temperatures of 700 °C, and 800 °C, it can be observed that its concentration remains constant along the length after initial production at the lower temperature, while some methane is converted to CO through SMR reaction at higher temperatures.

Conclusions

In the increasing demand for clean energy, the importance of solid oxide fuel cells (SOFCs) lies in their high efficiency and fuel flexibility. The two-stage process of reforming hydrocarbon fuels to hydrogen and then to power with water as a by-product, is a key aspect of SOFCs. The present work involves the development of an SOFC model with direct internal reforming based on a validated reformer model. Through detailed investigation, it is concluded that with the increasing operating temperature, the reaction rates of ethanol decomposition and WGS reactions increase exponentially around 600 K, while methane steam reforming shows an exponential increase after approximately 850 K. Species concentration profiles along the channel length confirm that ethanol decomposition occurs near the front and H_2 yield increases along the reactor length due to water gas shift and methane steam reforming reactions. The polarization curve demonstrates that higher temperatures result in increased hydrogen yield, higher Nernst voltage, and improved performance at higher current densities primarily due to reduced ohmic resistance. With increasing current density at fixed feed flow rate, hydrogen, and CO fractions decrease, while CO_2 fraction increases due to the water gas shift reaction. In contrast, the CH_4 concentration remains relatively unchanged at the given temperature due to the slow methane reforming reaction.

Author contributions

The authors confirm contribution to the paper as follows: study conception and design: Sarkar B, Gundlapally S; analysis and interpretation of results: Hariharan D, Gundlapally S; draft manuscript preparation: Hariharan D, Gundlapally S. All authors reviewed the results and approved the final version of the manuscript.

Data availability

The datasets generated during and/or analyzed during the current study are available from the corresponding author on reasonable request.

Conflict of interest

The authors declare that they have no conflict of interest.

Dates

Received 30 April 2024; Revised 24 June 2024; Accepted 15 July 2024; Published online 13 August 2024

References

1. Office of Energy Efficiency & Renewable Energy. n.d. *Fuel cells*. www.energy.gov/eere/fuelcells/fuel-cells
2. International Energy Agency. 2022. *Global Hydrogen Review 2022*. Technical Report. International Energy Agency, Paris. https://iea.blob.core.windows.net/assets/c5bc75b1-9e4d-460d-9056-6e8e626a11c4/GlobalHydrogenReview2022.pdf
3. Zhang M, Yang X. 2022. The regulatory perspectives to China's emerging hydrogen economy: characteristics, challenges, and solutions. *Sustainability* 14(15):9700
4. U.S. Energy Information Administration (EIA). 2023. *Hydrogen explained: production of hydrogen*. www.eia.gov/energyexplained/hydrogen/production-of-hydrogen.php
5. U.S. Energy Information Administration (EIA). 2024. *Biofuels explained: ethanol*. www.eia.gov/energyexplained/biofuels/ethanol-supply.php
6. Nanda S, Rana R, Zheng Y, Kozinski JA, Dalai AK. 2017. Insights on pathways for hydrogen generation from ethanol. *Sustainable Energy & Fuels* 1(6):1232–45
7. Huber GW, Iborra S, Corma A. 2006. Synthesis of transportation fuels from biomass: Chemistry, catalysts, and engineering. *Chemical Reviews* 106(9):4044–98
8. Idriss H. 2004. Ethanol reactions over the surfaces of noble metal/cerium oxide catalysts. *Platinum Metals Review* 48(3):105–15
9. Ye XF, Wang SR, Hu Q, Wang ZR, Wen TL, et al. 2009. Improvement of multi-layer anode for direct ethanol solid oxide fuel cells. *Electrochemistry Communications* 11(4):823–26
10. Ye XF, Wang SR, Wang ZR, Hu Q, Sun XF, et al. 2008. Use of $La_{0.75}Sr_{0.25}Cr_{0.5}Mn_{0.5}O_3$ materials in composite anodes for direct ethanol solid oxide fuel cells. *Journal of Power Sources* 183(2):512–17
11. Jiang Y, Virkar AV. 2001. A high performance, anode-supported solid oxide fuel cell operating on direct alcohol. *Journal of the Electrochemical Society* 148(7):A706
12. Wang W, Wang F, Ran R, Park HJ, Jung DW, et al. 2014. Coking suppression in solid oxide fuel cells operating on ethanol by applying pyridine as fuel additive. *Journal of Power Sources* 265:20–29
13. Wang W, Chen Y, Wang F, Tade MO, Shao Z. 2015. Enhanced electrochemical performance, water storage capability and coking resistance of a $Ni+BaZr_{0.1}Ce_{0.7}Y_{0.1}Yb_{0.1}O_{3-\delta}$ anode for solid oxide fuel cells operating on ethanol. *Chemical Engineering Science* 126:22–31
14. Lo Faro M, Reis RM, Saglietti GGA, Oliveira VL, Zignani SC, et al. 2018. Solid oxide fuel cells fed with dry ethanol: The effect of a perovskite protective anodic layer containing dispersed Ni-alloy @ FeOx core-shell nanoparticles. *Applied Catalysis B: Environmental* 220:98–110
15. Ye XF, Wang SR, Hu Q, Chen JY, Wen TL, et al. 2009. Improvement of Cu–CeO_2 anodes for SOFCs running on ethanol fuels. *Solid State Ionics* 180(2-3):276–81
16. García VM, López E, Serra M, Llorca J. 2009. Dynamic modeling of a three-stage low-temperature ethanol reformer for fuel cell application. *Journal of Power Sources* 192(1):208–15
17. Ulejczyk B, Jóźwik P, Nogal Ł, Młotek M, Krawczyk K. 2022. Efficient conversion of ethanol to hydrogen in a hybrid plasma-catalytic reactor. *Energies* 15(9):3050
18. Ni M, Leung DYC, Leung MKH. 2007. A review on reforming bio-ethanol for hydrogen production. *International Journal of Hydrogen Energy* 32(15):3238–47
19. López E, Divins NJ, Anzola A, Schbib S, Borio D, et al. 2013. Ethanol steam reforming for hydrogen generation over structured catalysts. *International Journal of Hydrogen Energy* 38(11):4418–28
20. Andersson M, Paradis H, Yuan J, Sundén B. 2011. Modeling analysis of different renewable fuels in an anode supported SOFC. *Journal of Fuel Cell Science and Technology* 8(3):031013
21. Dokmaingam P, Assabumrungrat S, Soottitantawat A, Laosiripojana N. 2010. Modelling of tubular-designed solid oxide fuel cell with indirect internal reforming operation fed by different primary fuels. *Journal of Power Sources* 195(1):69–78
22. Laosiripojana N, Assabumrungrat S. 2007. Catalytic steam reforming of methane, methanol, and ethanol over Ni/YSZ: The possible use of these fuels in internal reforming SOFC. *Journal of Power Sources* 163(2):943–51
23. Augusto BL, Noronha FB, Fonseca FC, Tabuti FN, Colman RC, et al. 2014. Nickel/gadolinium-doped ceria anode for direct ethanol solid oxide fuel cell. *International Journal of Hydrogen Energy* 39(21):11196–209
24. Sarruf BJM, Hong JE, Steinberger-Wilckens R, de Miranda PEV. 2020. Ceria-Co-Cu-based SOFC anode for direct utilisation of methane or ethanol as fuels. *International Journal of Hydrogen Energy* 45(8):5297–308
25. Hariharan D, Chhatija H, Brown J, Gundlapally S. 2024. *Modeling and analysis of the hydrogen production via steam reforming of ethanol, methanol, and methane fuels*. SAE Technical Paper Series. Detroit, Michigan, USA: WCX SAE World Congress. DOI: 10.4271/2024-01-2179
26. Dogdibegovic E, Fukuyama Y, Tucker MC. 2021. Ethanol internal reforming in solid oxide fuel cells: a path toward high performance metal-supported cells for vehicular applications. *Journal of Power Sources* 449:227598
27. Gundlapally SR, Balakotaiah V. 2011. Heat and mass transfer correlations and bifurcation analysis of catalytic monoliths with developing flows. *Chemical Engineering Science* 66(9):1879–92
28. Shah RK, London AL. 1978. Laminar flow forced convection in ducts: a source book for compact heat exchanger analytical data. New York: Academic Press. https://searchworks.stanford.edu/view/729747
29. Gundlapally SR, Papadimitriou I, Wahiduzzaman S, Gu T. 2016. Development of ECU capable grey-box models from detailed models — application to a SCR reactor. *Emission Control Science and Technology* 2(3):124–36
30. Gundlapally SR, Dudgeon R, Wahiduzzaman S. 2018. Efficient solution of washcoat diffusion-reaction problem for real-time simulations. *Emission Control Science and Technology* 4(2):90–102
31. Jiang Y, Virkar AV. 2003. Fuel composition and diluent effect on gas transport and performance of anode-supported SOFCs. *Journal of the Electrochemical Society* 150(7):A942
32. Andersson M, Yuan J, Sundn B. 2012. SOFC modeling considering electrochemical reactions at the active three phase boundaries. *International Journal of Heat and Mass Transfer* 55(4):773–88